Alignment effects in electron capture from D_2^+ molecular ions by Ar^{2+}, N^{2+}, and He^{2+}

I. Reiser* and C. L. Cocke*
J. R. MacDonald Laboratory, Department of Physics, Kansas State University, Manhattan, Kansas 66506, USA

H. Bräuning
Institut für Kernphysik, Strahlenzentrum, Justus-Liebig Universität Gießen, Gießen, Germany
(Received 13 February 2003; published 30 June 2003)

We have studied collisions between D_2^+ molecular ions and doubly charged projectiles at collision velocities ranging from 0.19 a.u. to 0.51 a.u. Using a molecular ion gives us the unique opportunity to investigate electron capture from a true one-electron, two-center target. The experimental results indicate that electron capture is preferred if the molecular axis is perpendicular to the collision velocity, independent of projectile and magnitude of collision velocity. We also present results from a theoretical model calculation. The calculation qualitatively supports the experimental findings, although some features in the calculation are not reproduced by the experiment. We discuss whether those features are natural.

DOI: 10.1103/PhysRevA.67.062718 PACS number(s): 34.70.+e, 34.50.Lf

I. INTRODUCTION

Electron capture from single-center targets in ion-atom collisions is rather well understood. For example, absolute capture cross sections for $p+H$ collisions are in agreement with theoretical calculations with less than 25% error over a wide range of collision energies (meV to MeV) [1]. Replacing the hydrogen atom with a hydrogen molecule as target changes the situation. The internuclear axis introduces an additional degree of freedom to the collision. To the extent that the electronic wave function can be represented as a linear combination of atomic orbitals, the amplitude for capture from such a two-center target can be thought of as linear combination of single-center amplitudes with a relative phase that depends on the vector internuclear distance. The situation is very similar to that of Young's two-slit interference experiment: the total amplitude for electron transfer is modulated according to the interference between the two amplitudes. This interference effect will manifest itself in the dependence of the transfer cross section on the alignment of the target molecule with respect to the beam direction.

The most convenient way to measure the molecular alignment dependence of a cross section for a collisionally induced electronic transition is to measure the vector momentum(a) of the dissociation fragments. Many experiments investigating the influence of the molecular axis alignment on the reaction have been carried out recently in photo- and collision-induced ionization of diatomic molecules [2–7]. To experimentally determine the alignment of the nuclear axis, most of these experiments take advantage of the recoil approximation [8]. If the fragmentation process is fast compared to the rotational and vibrational motion of the parent molecule, the fragments produced in the collision recoil along the internuclear axis. Measuring the relative velocity vector of the two fragments reveals the alignment of the internuclear axis when the molecule breaks up. This approach is only applicable to dissociative final states.

When applied to electron capture from neutral H_2 molecules, this approach requires that a two-electron process take place. If one electron is captured, the other electron must also be excited/ionized in order to populate the requisite dissociative final state. The dependence of electron capture on the alignment of the target molecular axis was measured by Cheng *et al.* [3] for electron capture from H_2 by fast O^{8+} projectiles, using the recoil method discussed above. Only the transfer ionization channel, which leads to removal of both electrons, was studied. Such a process is much more complex to analyze theoretically than a clean single capture process, and requires that broad generalizations about the role of the excitation/ionization of the second electron be made in order to compare the results of the experiment with theory [9–13].

In this study, the target is a D_2^+ molecular ion. Since this is a true one-electron molecular target, the two-center aspect can be investigated unambiguously without the complication of the second electron. After capturing the electron from the target, the two remaining D^+ fragments recoil from each other, allowing one to determine the molecular axis alignment through measuring the relative recoil velocity of the fragments. We have studied the dependence of single capture on the alignment between beam and the molecular axis for the following collision systems:

$$Ar^{2+}+D_2^+ \rightarrow Ar^+ + 2D^+ v_{coll}=0.19 \text{ a.u.}, \quad (1)$$

$$N^{2+}+D_2^+ \rightarrow N^+ + 2D^+ v_{coll}=0.23 \text{ a.u.}, \quad (2)$$

$$He^{2+}+D_2^+ \rightarrow He^+ + 2D^+ v_{coll}=0.4 \text{ a.u.}, \quad (3)$$

$$He^{2+}+D_2^+ \rightarrow He^+ + 2D^+ v_{coll}=0.51 \text{ a.u.} \quad (4)$$

The Ar^{2+} and N^{2+} capture populate dominantly the $3p$ and $2p$ orbitals on the final ion, respectively. For He^{2+}, the dominant capture is to $n=2$ [14]. The first two collision systems are very similar in Q value, which is very small, $Q=-0.3$ eV for the N^{2+} projectile and $Q=-2.3$ for the

*Present Address: Department of Radiology, The University of Chicago, Chicago, IL 60637, USA.

Ar^{2+} projectile. The last two collision systems have the same projectile, at two velocities. For the He^{2+} projectiles, $Q = -16.3$ eV, resulting in a smaller capture cross section but larger expected alignment effect, as discussed below.

II. THEORETICAL MODEL

Several groups have established models for ion-molecule collisions [12,13,15,16]. We have previously described the application of a collision model developed by Shingal and Lin [16] to calculate the total charge transfer cross sections for He^{2+} and Ar^{2+} on H_2^+ [14]. In this paper, we use this model to calculate the dependence of the capture cross section on θ, which is the alignment of the molecular axis with respect to the projectile velocity vector. Since a detailed description of the approach is given in Ref. [14], we summarize here only the major features. In this model, the scattering amplitudes for the ion-molecule collision system are constructed from the scattering amplitudes of the respective ion-atom collision system through coherent superposition:

$$a_{fi} = \frac{1}{\sqrt{2}}\left\{ a(\vec{b}_A) + a(\vec{b}_B)\exp\left[-iR\cos(\theta)\left(\frac{v}{2} - \frac{\omega}{v}\right)\right]\right\}, \tag{5}$$

where $a(\vec{b}_A)$ and $a(\vec{b}_B)$ are the scattering amplitudes of the atomic collision system consisting of the projectile and one molecular constituent (A) or (B), R is the internuclear separation in the molecular ion, θ is the angle between projectile velocity and internuclear axis, v is the collision velocity, and ω is the energy difference of initial and final state. The scattering amplitudes $a(\vec{b})$ of the atomic X^{2+}-D collision system (X=Ar, N, He) are obtained through a close-coupling calculation, as described in Ref. [17]. The internuclear separation R of the D_2^+ molecular ion is 2 a.u. The ground-state energy E_{1s} at this R is calculated to be 1.13 a.u., using a linear combination of atomic orbitals approach with variable effective charge [18]. From the molecular scattering amplitudes, cross sections are derived through

$$\sigma_{tot}(\theta) = \int |a_{fi}(\vec{b})|^2 d\vec{b}. \tag{6}$$

Because of the molecular target, the collision system exhibits no cylindrical symmetry and the impact parameter integration needs to be carried out in two dimensions. The total cross section varies as a function of θ. Since $\cos(\theta)$ varies between -1 and 1, the magnitude of the variation is determined by the factor $\Phi_0 = (v/2 - \omega/v)$, which, in turn, depends on the reaction of Q value (ω), and on the collision velocity v. Varying those parameters changes the alignment effect.

The factor Φ_0 is plotted on the bottom graph of Fig. 1, for the three projectile's Q values, as a function of collision velocity. Only for the He^{2+} projectile at low velocity is much variation in the alignment effect expected. The alignment dependent cross sections for the He^{2+} projectile are plotted as a polar plot in the inset of the top part of the figure. Also

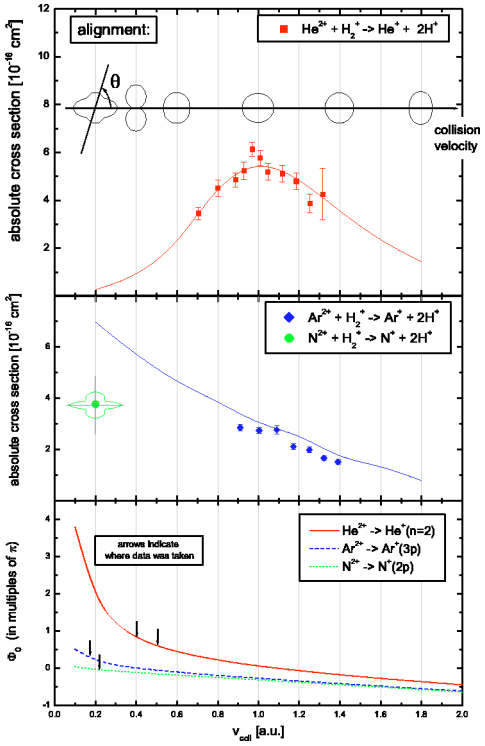

FIG. 1. (Color online) Theoretical results for the electron capture cross section from H_2^+ molecular ions by He^{2+} (top) and Ar^{2+}, N^{2+} (middle) as a function of collision velocity. The top and middle insets show polar plots of the *e*-capture CS as a function of alignment angle. The bottom graph shows the phase factor Φ_0 for the three projectiles as a function of collision velocity.

shown are the total cross section for all the projectiles used in this experiment, as a function of collision velocity. For He^{2+} projectiles at small collision velocities, where the alignment dependence varies rapidly with velocity, the total cross section is very small.

III. EXPERIMENTAL APPROACH

A. Apparatus

The experiment was carried out on the 90° crossed beams ion-ion collision apparatus at the JR MacDonald laboratory (Fig. 2 and [17]). The doubly charged projectiles were produced in a 4.5 GHz ECR ion source and the D_2^+ molecular ions were created in a Penning ion source. The beams collided in a collision region where the background pressure was kept in the low 10^{-10} Torr range. The collision region, which has a length of 38 cm, was held at high voltage. After collision, the charge-changed products were separated from the parent ion beam by magnets and energy analyzed by electrostatic deflectors. The electrostatic deflectors allowed only charge-exchange products, emerging from the collision region to follow a trajectory toward the position-sensitive MCP detector. For the initially doubly charged projectiles (ECR beam), which became singly charged in the capture, a MCP detector in conjunction with a wedge-and-strip anode was used. For detection of the molecular fragments, a MCP detector with a delay-line anode was used, which allowed us

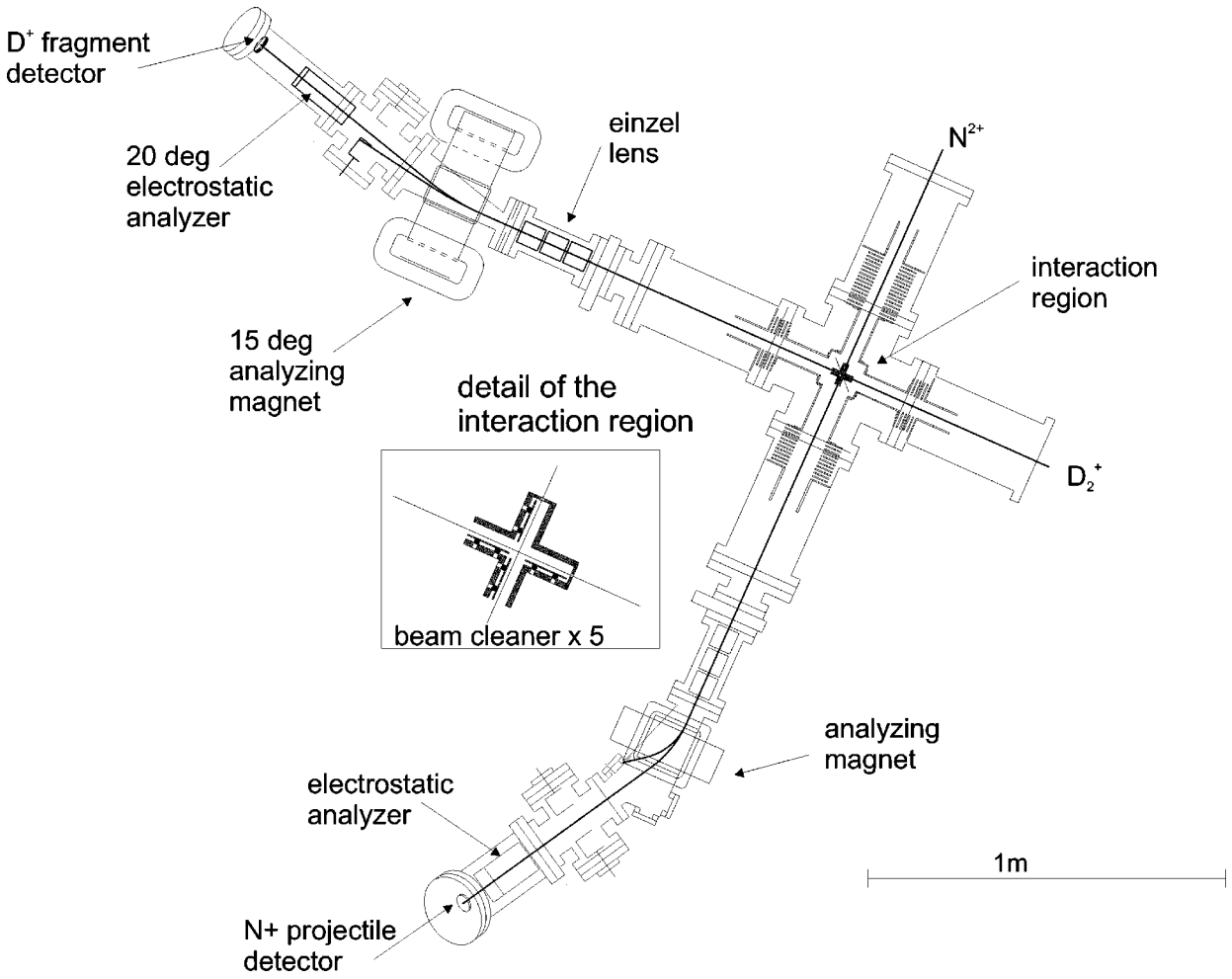

FIG. 2. The KSU ion-ion collision facility.

to record the times and positions of both particles simultaneously [19]. The dead time of this detector was about 15 ns, which is much shorter than the maximum flight time difference of two molecular fragments of 150 ns. The true ion-ion collision products were identified through a triple coincidence, requiring two hits on the delay-line detector within 400 ns, and a third hit on the wedge-and-strip detector. With two coincidence windows of 400 ns and 2 μs, the random rate for the triple coincidence was of the same order as the true rate, 0.1 Hz. Typical beam currents were 50 nA for the projectile ECR beam and 20 nA for the molecular beam. Detection of all molecular fragments was ensured by an arrangement of two ion-optical lenses. The lens voltages were set such that momentum focusing of the molecular fragments was achieved, which means that particles emerging from the beam intersection with equal velocity vectors are projected onto the same detector position, regardless of where they originated from within the collision volume. Detector positions were calibrated to scattering angle by deflecting a D^+ test beam at the collision region. The calibration procedure as well as the corrections for the electrostatic and magnetic analyzers are described in detail in Refs. [20,21].

B. Background reduction

In order to further reduce background events, the projectile beam (i.e., the doubly charged beam) was cleaned prior to intersecting the molecular ion beam, and partially separated within the collision region by means of two electrostatic deflectors. Those deflectors were placed within 1 cm of the beam intersection. The voltages applied were small (typically less than 100 V); different charge states were merely tagged with slightly different scattering angles in order to be able to fully collect the parent ion beam further downstream. On the position-sensitive detector, the different charge states produced beam spots at different locations. Particles resulting from collisions with background gas were either blocked out using a beam block or through software in the data analysis. This measure resulted in a background reduction of about a factor of 10. The molecular ion beam could not be cleaned in this way, since the angle used to tag the beam was of the order of the expected scattering angles of the molecular fragments. The rate of true events was 0.1 Hz (for the Ar^{2+} and N^{2+} projectiles) and 0.02 Hz (for the He^{2+} projectile at $v_{coll}=0.4$ a.u.). With those measures in place, the real-to-random ratio was between 2.5 (for the Ar^{2+} projectile) and

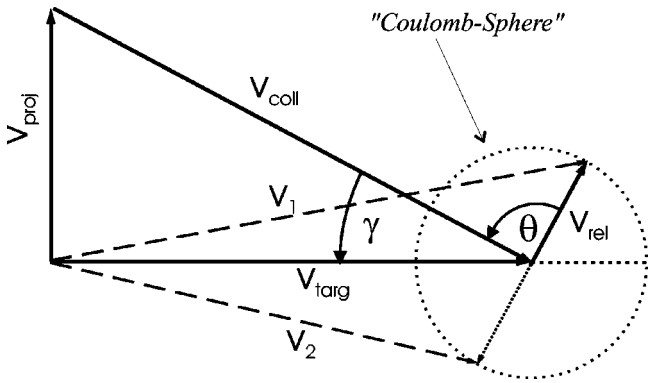

FIG. 3. Collision geometry for a crossed-beam experiment with an expanding Coulomb sphere in one of the beams.

0.4 (for the He^{2+} projectile). The running time to accumulate 20 000–50 000 true events was 5–9 days.

IV. DATA ANALYSIS

Collision kinematics

In a crossed-beam experiment, the collision velocity is a vector lying in the plane spanned by the two ion-beam directions. Its orientation with respect to the two beams depends on the relative magnitude of the beam velocities. This is shown in Fig. 3, where $\mathbf{v}_{proj}$ is the projectile beam velocity, $\mathbf{v}_{targ}$ is the molecular ion-beam velocity, $\mathbf{v}_{coll}$ is the the collision velocity, and γ is the angle between the collision velocity and the molecular ion-beam direction. The value of these parameters for each collision system is tabulated in Table I.

In the collision, the molecular ion breaks into its two constituents. The fragment center of mass travels along the parent ion-beam direction. The fragment velocities with respect to their center of mass lie on the three-dimensional Coulomb sphere. The fragment velocities with respect to the collision are denoted by $\mathbf{v}_1$ and $\mathbf{v}_2$. Once the electron is captured from the molecular ion, the fragments recoil along the internuclear axis. Thus, the molecular alignment during the collision can be revealed by determining the relative velocity of the two fragments, $\mathbf{v}_{rel}=(\mathbf{v}_1-\mathbf{v}_2)/2$. The vector $\mathbf{v}_{rel}$ was deduced from the measured positions and times of impact of the ions on the delay-line detector [20,21]. The alignment angle θ is then deduced as the angle between $\mathbf{v}_{rel}$ and the collision velocity $\mathbf{v}_{coll}$.

TABLE I. Kinematic quantities of the four projectile ions colliding at right angles with a 3.1-keV D_2^+ ion beam [$v=3.86(5)$ m/s].

Projectile ion	Projectile energy (keV)	Projectile velocity (10^5 m/s)	Collision velocity (10^5 m/s)	(a.u.)	γ (deg)
Ar^{2+}	5.2	1.58	4.17	0.19	22
N^{2+}	7.2	3.14	4.98	0.23	39
He^{2+}	14.2	8.25	9.11	0.42	65
He^{2+}	23.2	10.5	11.19	0.51	70

V. RESULTS AND DISCUSSION

Figure 4 shows the slices of the resulting Coulomb sphere, presented as density plots of the measured values of the laboratory momenta of the fragments $\mathbf{k}_1$ and $\mathbf{k}_2$, where $\mathbf{k}_1=m\mathbf{v}_{rel}$ and $\mathbf{k}_2=-m\mathbf{v}_{rel}$. In this figure the z axis is defined to be in the direction perpendicular to the face of the detector and the x axis is defined to be the detector position coordinate that lies in the plane defined by the relative velocities of the two ion-beams; that is, the z direction is the time direction of the fragments and the x the horizontal position direction on the detector (see Fig. 3). The slices shown in Fig. 4 are formed by requiring that the absolute value of the y component of the momentum difference $\mathbf{k}_1-\mathbf{k}_2$ be less than 10 a.u. The radius of this sphere is an indication of the internuclear distance from which the singly charged deuterons began their explosion following the capture. In this case, we expect that this value will approximately reflect the motion of the wave packet formed initially in the ion source from D_2 at an internuclear distance of 1.4 a.u., but after it has oscillated for a long enough time in the gerade potential curve of the D_2^+ molecule that the coherence of the vibrational states in this potential has been lost. If the resulting wave packet is reflected onto the D^+-D^+ potential curve, it results in a broad distribution of release energies between 10 and 20 eV. On this basis, one would expect a rather broad Coulomb explosion sphere with a radius in k_1 (or k_2) of approximately 45 a.u. This expectation is consistent with the data of Fig. 4.

The direction of the vector $\mathbf{v}_{coll}$, which lies in the x-z plane, is indicated in Fig. 4 for each collision system. If there were no dependence of the cross section on θ, the slices would be expected to be uniformly populated rings. But they are not. There is a clear propensity for the events to lie preferentially at right angles to $\mathbf{v}_{coll}$, indicating that the capture cross section is larger for the molecules that are perpendicular to $\mathbf{v}_{coll}$ than for those along $\mathbf{v}_{coll}$. The gap along the $\mathbf{k}_z^{lab}$ axis is caused by the limited pulse-pair resolution of the multihit detector.

The angular distributions extracted from the two-dimensional plots of Fig. 4 are shown in Fig. 5. The angle on the bottom axis of the plot is the angle in the laboratory system and the angle on the top of each plot is the angle with respect to each collision velocity. The data are unreliable in several angular ranges. The gaps around $\theta_{lab}=0$ and 180° are caused by the pulse-pair resolution of the detector; data are missing here. Data points plotted without error bars occur in regions where a high density of background events hit the detector. These events result from collision-induced dissociations of molecular ions colliding with rest gas constituents; therefore, the scattering angles of those fragments are much smaller than that of the molecular fragments resulting from the Coulomb explosion. Such high background regions are plagued by large detector efficiency and background subtraction uncertainties and are excluded from further analysis.

Figure 6 shows the angular distribution in the collision system's center of mass, purged of the unreliable data regions. Those distributions were obtained from Fig. 5 by symmetrization about each collision velocity, a procedure that

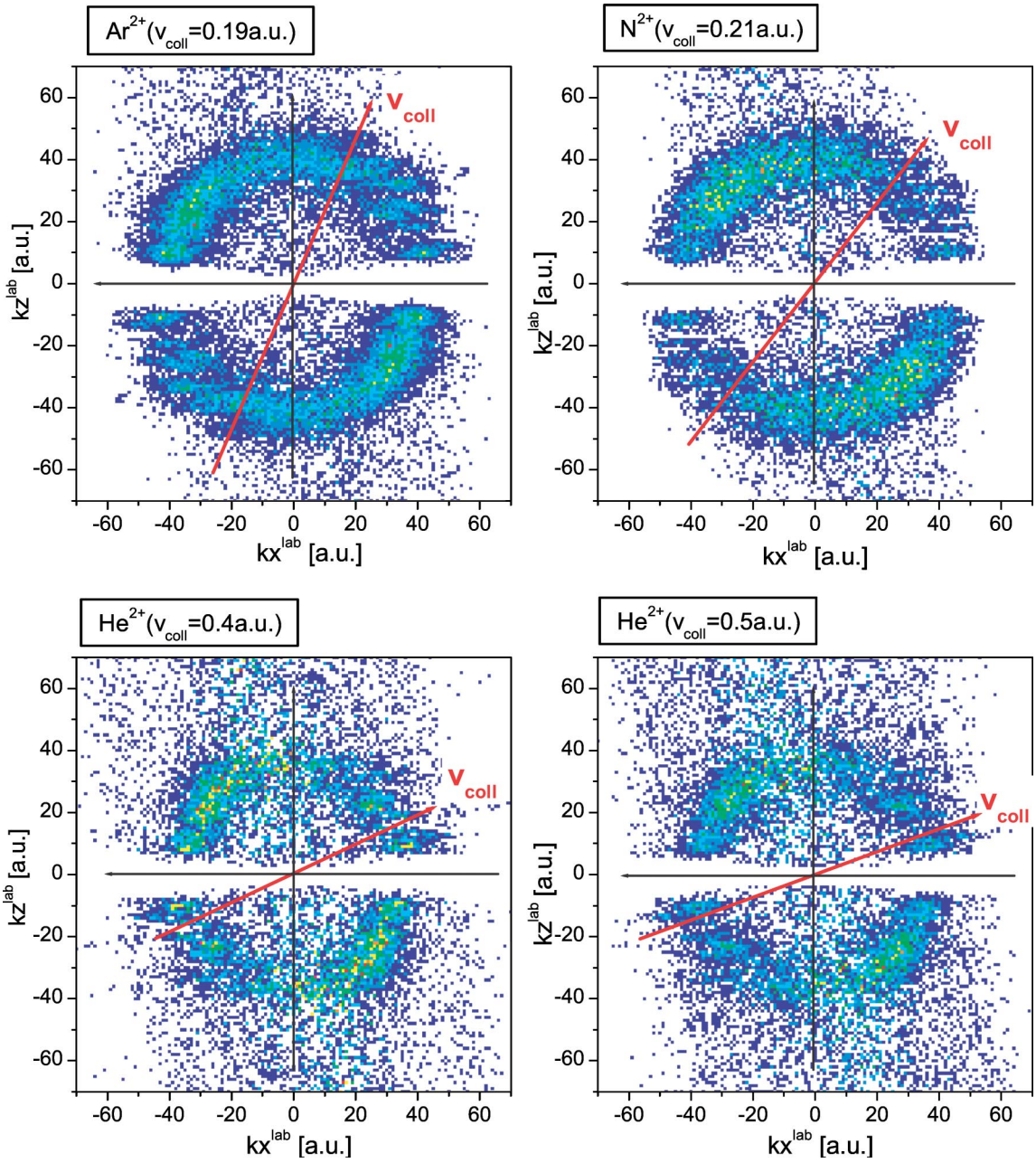

FIG. 4. (Color online) Slices of the Coulomb sphere in the $\mathbf{k}_x$-$\mathbf{k}_z$ plane. In each frame, $\mathbf{v}_{proj}$ is pointing along the negative $\mathbf{k}_x$ axis, and $\mathbf{v}_{targ}$ is pointing along the positive $\mathbf{k}_z$ axis. The data shown were calibrated and the analyzer distortions were corrected for.

produces a complete dataset in spite of the exclusion of angular regions in Fig. 5. The right-hand column in Fig. 6 shows the results from the theoretical calculation, as described in Sec. II for the same collision systems. Both the data and the theory agree that the cross section is enhanced when the molecule is perpendicular to the beam direction. We interpret this enhancement as due to the constructive interference between capture from the two centers of the molecule, which occurs when the molecule is in this alignment. This interpretation is supported by the calculation for which the maximum comes from this effect. Other aspects of the model are not seen in the data, however. For the Ar^{2+}-D_2^+ and N^{2+}-D_2^+ collision systems, the calculated angular distributions show spikes at 0 and 180°, which are clearly not seen in the experimental data. These spikes originate in the model from the spatial overlap, in the integral of Eq. (6), of $a(\vec{b}_A)$ and $a(\vec{b}_B)$ of Eq. (5). This overlap maximizes when the molecule is aligned along the beam. The effect is strongest for a small longitudinal momentum transfer, for which the phase factor in Eq. (5) is nearly unity. This is the case for the two nearly resonant capture cases, but not for the He^{2+} projectile. It appears that this is an artifact of the model, not to be seen in nature. In addition, the size of the enhancement at $\theta = 90°$ is not particularly well reproduced by the model. Because the longitudinal momentum transfer is largest for the endoergic capture by He^{2+}, the phase factor in Eq. (5) is

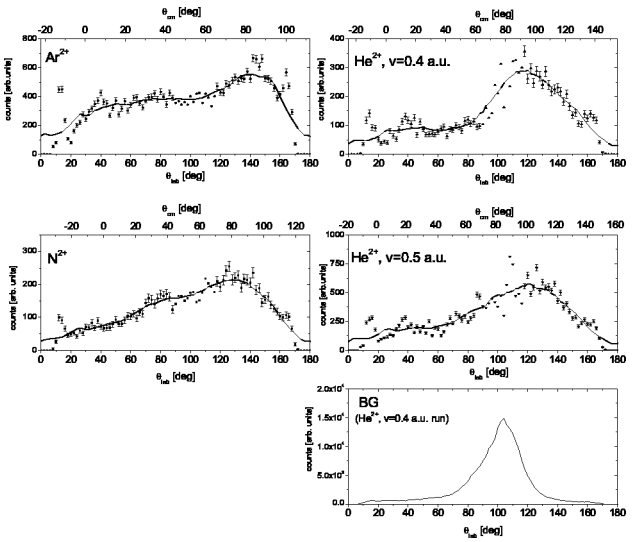

FIG. 5. Alignment dependence of electron capture from D_2^+ molecular ions by Ar^{2+}, N^{2+}, and He^{2+} projectiles. In each frame, the alignment angle *relative to the molecular ion-beam* is plotted on the bottom axis, and the alignment angle *relative to the collision velocity* is plotted on the top axis. The relative positions of top and bottom axes differ for each collision system. BG: angular distribution of the background collisions.

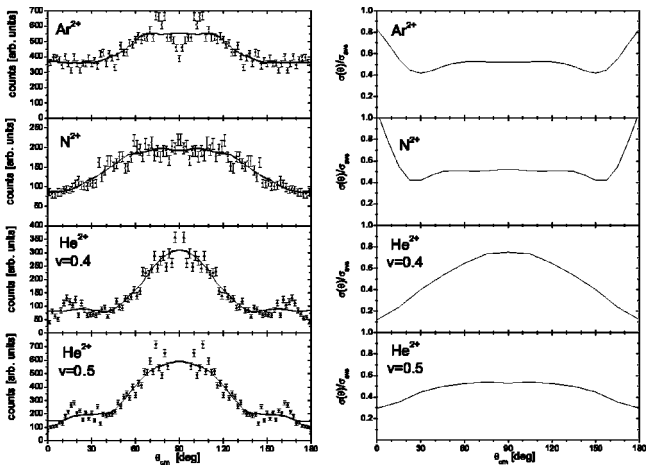

FIG. 6. Alignment dependence of electron capture from D_2^+ molecular ions by Ar^{2+}, N^{2+}, and He^{2+} projectiles. Experimental data (left) in comparison to the theoretical calculation (right). The line through the experimental data points is a smooth of the data.

most strongly angle dependent for this case. Thus one would expect to see a more marked θ dependence for this case than for the Ar^{2+} and N^{2+} cases. The experimental data support this qualitatively to some extent, but there is no real quantitative agreement between model and experiment on this issue.

VI. SUMMARY AND CONCLUSION

In summary, we have determined the alignment dependence of electron capture from D_2^+ by various projectile ions at varying collision velocities. The target system is a true one-electron molecule, and the capture involves only this active electron in all cases. For the case of the He^{2+} projectile, the collision system is a true one-electron system, the cleanest for which this kind of investigation has ever been made. The most important feature of the results is the enhancement of capture, for all collision systems, when the molecular ion is aligned perpendicular to the collision velocity. We believe the major physical reason for this is that the amplitudes for capture from the two centers of the molecule add exactly in phase for this alignment of the molecule. This interpretation is supported by a comparison of the data with the results of a model calculation that treats capture from molecular target as the coherent superposition of a, electron capture from two atomic targets.

ACKNOWLEDGMENTS

We would like to thank C. D. Lin, I. Ben-Itzhak, and E. Salzborn for useful discussions. This work was supported by the Chemical Sciences, Geosciences and Biosciences Division, Office of Basic Energy Sciences, Office of Science, U.S. Department of Energy, and the Alexander von Humboldt Foundation (H.B.).

[1] ALADDIN database, www-amdis.iaea.org/aladdin/html, maintained by J. A. Stephens at the International Atomic Energy Agency (www.iaea.org).
[2] A.K. Edwards, R.M. Wood, M.A. Mangan, and R.L. Ezell, Phys. Rev. A **46**, 6970 (1992).
[3] S. Cheng, C.L. Cocke, V. Frohne, E.Y. Kamber, J.H. McGuire, and Y. Wang, Phys. Rev. A **47**, 3923 (1993).
[4] U. Werner, N.M. Kabachnik, V.N. Kondratyev, and H.O. Lutz, Phys. Rev. Lett. **79**, 1662 (1997).
[5] R. Dörner *et al.*, Phys. Rev. Lett. **81**, 5776 (1998).
[6] B. Siegmann, U. Werner, Z. Kaliman, N.M. Kabachnik, and H.O. Lutz, Phys. Rev. A **65**, 010704(R) (2001).
[7] N. Stolterfoht *et al.*, Phys. Rev. Lett. **87**, 023201 (2001).
[8] R.N. Zare, Wiss. Z.-Karl-Marx-Univ. Leipzig, Mol. Photochem. **4**, 1 (1972).
[9] M. Kimura, Phys. Rev. A **32**, 802 (1985).
[10] M. Kimura, S. Chapman, and N.F. Lane, Phys. Rev. A **33**, 1619 (1986).
[11] N.C. Deb, A. Jain, and J.H. McGuire, Phys. Rev. A **38**, 3769 (1988).
[12] Y.D. Wang, J.H. McGuire, and R.D. Rivarola, Phys. Rev. A **40**, 3673 (1989).
[13] Y.D. Wang and J.H. McGuire, Phys. Rev. A **44**, 367 (1991).
[14] H. Bräuning, I. Reiser, A. Diehl, A. Theiß, E. Sidky, C.L. Cocke, and E. Salzborn, J. Phys. B **34**, L321 (2001).
[15] T.F. Tuan and E. Gerjuoy, Phys. Rev. **117**, 756 (1960).

[16] R. Shingal and C.D. Lin, Phys. Rev. A **40**, 1302 (1989).
[17] C.Y. Chen, C.L. Cocke, J.P. Giese, F. Melchert, I. Reiser, M. Stockli, E. Sidky, and C.D. Lin, J. Phys. B **34**, 469 (2001).
[18] J.P. Lowe, *Quantum Chemistry* (Academic Press, New York, 1993).
[19] I. Ali *et al.*, Nucl. Instrum. Methods Phys. Res. B **149**, 490 (1999).
[20] I. Reiser, Ph.D. thesis, Kansas State University, 2002 (unpublished).
[21] I. Reiser and C.L. Cocke, Nucl. Instrum. Methods Phys. Res. B **205**, 614 (2003).